**Advances in Concrete Construction**, *Vol. 20, No. 5 (2025) 363-381*
https://doi.org/10.12989/acc.2025.20.5.363


# Optimal design of CFRP plates for strengthening RC flat slab-column connections using GWO algorithm

Zana Kohneposhi, Hadi Azizian*, Omid Hadad and Seyed Jamil Ghaderi

*Department of Civil Engineering, Mah.C., Islamic Azad University, Mahabad, Iran*

(*Received August 3, 2023, Revised March 27, 2025, Accepted July 29, 2025*)

**Abstract.** The present research evaluated the effect of carbon-fiber-reinforced polymer (CFRP) plates in strengthening reinforced concrete (RC) flat slab-column connections under punching shear and seismic loading conditions and proposed an optimal design for CFRP plates in these connections. To this end, comprehensive parametric studies were performed in the ABAQUS finite element software using 33 different models incorporating various values of the 5 main variables, namely loading conditions, number of fiber layers, orientation, thicknesses, and dimensions of the CFRP plate. The numerical model was validated via experimental tests of the laboratory model. In addition, an optimal design model for CFRP plates was developed using the gray wolf optimization (GWO) algorithm. The main objective of the optimization model was to reduce damage in the slab-column connection under loading. The optimal values of the geometric parameters of the CFRP plates retrofitted in the RC slab-column connection were obtained by simultaneous computations performed by MATLAB and ABAQUS software. The results along with the CFRP optimization model developed using GWO can be used in practice to design CFRP plates optimally for reinforcement purposes.

**Keywords:** CFRP; concrete slab; GWO; optimal design; RC slab-column connection seismic behavior; seismic behavior

## 1. Introduction

Slab-column connections in reinforced concrete (RC) flat slabs are recognized as critical zones in the structural design of concrete buildings. These regions are subjected to concentrated flexural and shear stresses which, in the absence of adequate strengthening, are highly susceptible to punching shear failure. Such failure can result in brittle and sudden collapse of floor systems (Al-Maliki *et al*. 2021, Abdulrahman and Aziz 2021). Among modern retrofitting techniques, the use of carbon fiber-reinforced polymer (CFRP) plates has emerged as a promising and cost-effective solution for enhancing the performance of these connections (Akhundzada *et al*. 2019, El-Mandouh *et al*. 2022). Due to their high strength-to-weight ratio, corrosion resistance, and ease of installation, CFRP plates have gained significant attention from researchers in the field of structural rehabilitation.

Several studies have evaluated the flexural and shear performance of RC slab-column connections strengthened with CFRP. Harajli and Soudki (2003), and Esfahani *et al*. (2009) demonstrated the effectiveness of CFRP in enhancing the punching shear resistance of interior slab-column joints. Moon *et al*. (2017) and Aman *et al*. (2020) reported improvements in load-carrying capacity and stiffness of CFRP-strengthened slabs. More recent research by Mukhtar and Lardhi (2024) highlighted the application of near-surface mounted (NSM) FRP bars in increasing punching resistance in recycled aggregate slabs. Additionally, Yagar *et al*. (2024) developed a comprehensive database to evaluate the applicability of ACI code equations in estimating the punching capacity of FRP-strengthened connections.

In the context of seismic loading, studies such as those by Liu *et al*. (2021), Daud *et al*. (2015), and Ma *et al*. (2020) have shown that CFRP retrofitting leads to reduced displacements, improved energy dissipation capacity, and enhanced cyclic behavior of slab-column joints. El-Mandouh *et al*. (2022) and Babiker *et al*. (2024) further examined the beneficial impact of CFRP on the seismic performance of slabs with openings.

To advance the efficiency of such strengthening techniques, various metaheuristic algorithms have been employed in the structural optimization domain. These include the Genetic Algorithm (GA), Particle Swarm Optimization (PSO), and more recently, the Grey Wolf Optimizer (GWO), which has proven to be highly effective in handling complex civil engineering optimization problems. Aidy *et al*. (2022) and Rady and Mahfouz (2022) applied GA to optimize structural layouts of RC slabs. Truong *et al*. (2022) leveraged machine learning techniques to model the punching capacity of FRP-reinforced slabs. Introduced by Mirjalili *et al*. (2014), the GWO algorithm has demonstrated significant capabilities in optimization tasks and has been applied successfully in several structural engineering studies (Emmanuel *et al*. 2022, Yin *et al*. 2021). Moreover, recent efforts by Truong *et al*. (2022) and

*Corresponding author, Ph.D., Professor,
E-mail: hadi.azizian@yahoo.com;
hadi.azizian@iau.ac.ir



ISSN: 2287-5301 (Print), 2287-531X (Online)

Babiker *et al*. (2024) have focused on employing machine learning and deep learning approaches to predict the punching behavior of FRP-strengthened slabs with higher precision.

Given the increasing vulnerability of aging concrete structures and the critical need for efficient and cost-effective retrofitting methods, the application of rigorous numerical modeling and advanced optimization strategies becomes imperative. This necessity is particularly pronounced in seismic-prone regions, where enhancing the structural integrity of slab-column connections is both an engineering and safety priority. Despite the extensive use of CFRP in practice, many design decisions are still based on empirical judgment or trial-and-error approaches, which may not yield structurally or economically optimal solutions.

A critical review of the literature reveals that:

- Comprehensive numerical and parametric investigations on the geometric design variables of CFRP plates under combined static and seismic loads are still lacking.
- There is a notable research gap in the integrated optimization of multiple design parameters (such as thickness, orientation, dimensions, and number of CFRP layers) using intelligent algorithms in conjunction with finite element modeling (FEM) for RC slab-column connections.

The present study addresses this research gap by developing a computational framework for the optimal design of CFRP plates in RC slab-column joints. The framework is based on nonlinear finite element simulations conducted in Abaqus and an optimization module built in MATLAB using the Grey Wolf Optimizer. The objective function is defined to minimize damage indices under both static and cyclic loading scenarios.

The key novelty of this research lies in the integration of FEM-based structural analysis with GWO-driven optimization to simultaneously determine the optimal combination of four critical design parameters: number of CFRP layers, fiber orientation, plate thickness, and plate dimensions. To the best of the authors' knowledge, this is the first study to propose a unified methodology for the geometric optimization of CFRP plates tailored for RC slab-column retrofitting, with high potential for practical engineering applications.

This paper is structured into four main sections. Section 2 outlines the materials and methods, including details of the experimental benchmark model, numerical modeling strategy using Abaqus, material properties, and the implementation of GWO in MATLAB. Section 3 presents the numerical results and optimization outcomes, including parametric analyses, performance evaluation of various CFRP configurations, and the derivation of the optimal CFRP design. Finally, Section 4 provides conclusions and recommendations for future research.

## 2. Materials and method

### *2.1 Specifications of the reference model*

In this research, the numerical model was implemented in Abaqus software. In order to calibrate the numerical models and validate their performance, they must be created based on the laboratory model and undergo verification-validation steps with respect to the experimental model. Accordingly, the numerical slab-column model was defined and implemented according to the empirical model of Hamoda and Hossain (2019), which consisted of a RC flat slab with base dimensions of 1000 mm × 1000 mm and a thickness of 100 mm and a concrete column with base dimensions of 100 mm × 100 mm and a height of 300

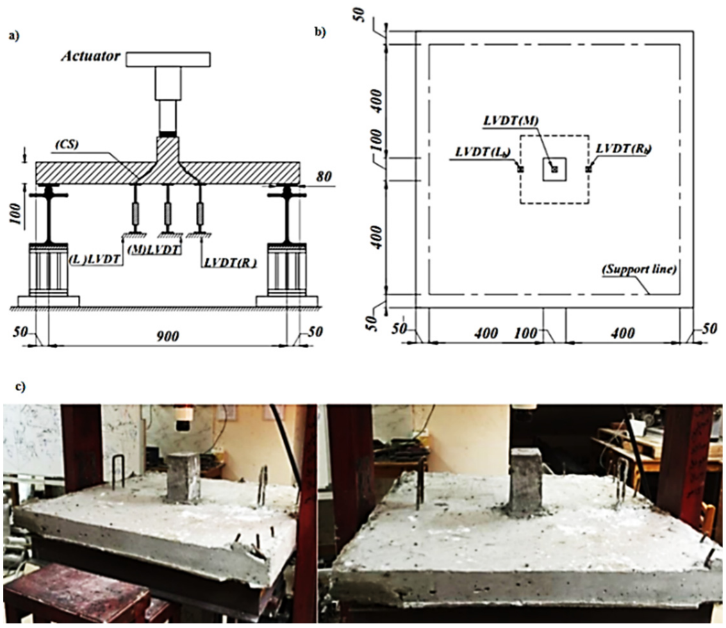


Fig. 1 Experimental setup and dimensions of the slab-column model: (a) schematic of the cross-section of the laboratory model; (b) plan of the laboratory model; (c) specimen and experimental setup (Hamoda and Hossain 2019)

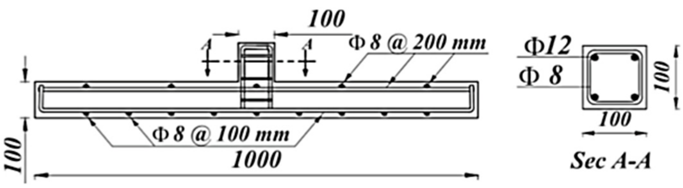


Fig. 2 Geometric specifications and reinforcement system configuration in the slab and column of the laboratory model

mm. Fig. 1 displays the schematic of the model and the experimental setup. In the laboratory model, 8-mm and 12-mm rebars were used in the column and 8-mm compressive and tensile rebars were used in the slab for reinforcement (Fig. 2).

The concrete in the experimental model had an average compressive strength of 32 N/mm$^2$ and tensile strength (based on 12 cylindrical specimens with dimensions of 150 mm × 300 mm) of 2.7 N/mm$^2$. The rebars used in the slab and column were made of steel with an elastic modulus of 200 N/mm$^2$, a yield strength of 365 N/mm$^2$, and an ultimate strength of 545 N/mm$^2$. In addition, the rebars had a nominal cross-sectional area of 199 mm$^2$. Table 1 summarizes the material properties extracted from the experimental benchmark used for validation, as described by Hamoda and Hossain (2019). For parameters not explicitly reported, standard values from literature and product datasheets were adopted. These values were used in the finite element model to ensure consistency and realism with the physical experiment.

### *2.2 Specifications of the numerical models*

In this research, a numerical model was created based on the properties and dimensions of the experimental model. Accordingly, a modulus of elasticity of E = 200.000 N/mm$^2$ and a Poisson's ratio of ν = 0.3 were considered as the elastic properties of steel for the numerical model. The plastic behavior of the steel is defined using its stress-strain curve (Fig. 3). Based on the laboratory model, the steel was found to have a yield stress of 365 N/mm$^2$ and an ultimate stress of 545 N/mm$^2$.

The properties of concrete were defined according to its elastic and plastic behavior (focusing mainly on the tensile and compressive damage). In this regard, the elastic properties of the concrete were taken to be a modulus of elasticity of E = 21.200 N/mm$^2$ and a Poisson's ratio of $\nu = 0.2$. Various techniques are used to define the specifications and plastic behavior of concrete under loading. Accordingly, the tensile and compressive behaviors of concrete are introduced, and the main parameters used to define its plastic behavior (damage) are defined in the software. The tensile and compressive behavior graphs of concrete are shown parametrically in Fig. 4.

Five groups of material data for concrete, including concrete damaged plasticity, compressive behavior, concrete compression damage, tensile behavior, and concrete tension damage must be specified in Abaqus in order to define the plastic behavior of concrete. Table 2 presents the plastic damage parameters of concrete used in the numerical model.

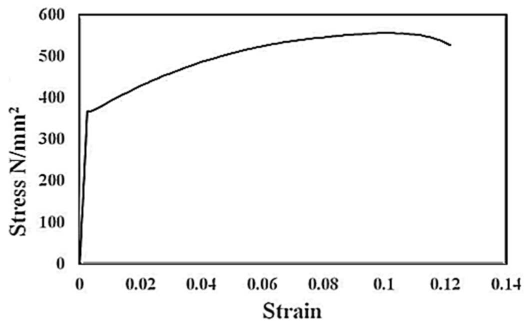


Fig. 3 Stress-strain curve of the steel used in the numerical model

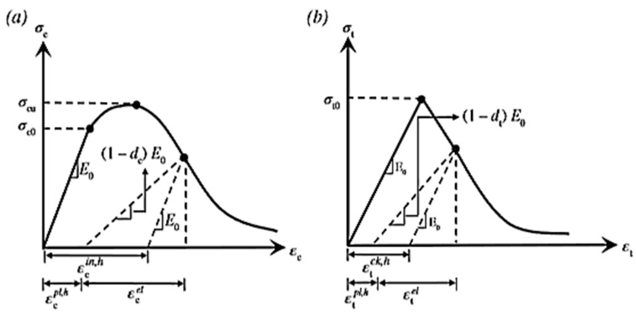


Fig. 4 Graph of the behavior of concrete (stress-strain) under (a) compression and (b) tension

Table 2 Plastic damage properties of concrete used in the numerical model

| Dilation angle | Eccentricity | fb0/fc0 | K | Viscosity parameter |
|---|---|---|---|---|
| 38 | 0.1 | 1.16 | 0.67 | 0.0009 |

The CFRP plates were defined using the shell (S4R) element in the numerical model. The Lamina type was used to define the elastic properties of the CFRP plates, and the Hashine Damage model was employed to define their damage properties. In addition, the damage evolution parameters in the CFRP plates were among the major specifications used to define the behavior of these plates in the numerical model. Table 3 shows the elastic parameters, the Hashine Damage model, and the damage evolution specifications in the numerical model of the CFRP plates. Finally, the composite material properties in Abaqus V. 2020 were used to define different layers and the specifications of the CFRP plates, such as thickness and fiber orientation in each layer.

Table 3 Specifications of the CFRP plates in the numerical model

<table>
<tr><th colspan="12">Elastic</th></tr>
<tr><td colspan="2">E1</td><td colspan="2">E2</td><td colspan="2">Nu12</td><td colspan="2">G12</td><td colspan="2">G13</td><td colspan="2">G23</td></tr>
<tr><td colspan="2">7000</td><td colspan="2">10000</td><td colspan="2">0.34</td><td colspan="2">8000</td><td colspan="2">4700</td><td colspan="2">8000</td></tr>
<tr><td colspan="2">Longitudinal tensile strength</td><td colspan="2">Longitudinal compressive strength</td><td colspan="2">Transverse tensile strength</td><td colspan="2">Transverse compressive strength</td><td colspan="2">Longitudinal shear strength</td><td colspan="2">Transverse shear strength</td></tr>
<tr><td colspan="2">1340</td><td colspan="2">1192</td><td colspan="2">19.6</td><td colspan="2">92.3</td><td colspan="2">51</td><td colspan="2">23</td></tr>
<tr><th colspan="12">Damage evolution</th></tr>
<tr><td colspan="3">Longitudinal tensile fracture energy</td><td colspan="3">Longitudinal compressive fracture energy</td><td colspan="3">Transverse tensile fracture energy</td><td colspan="3">Transverse compressive fracture energy</td></tr>
<tr><td colspan="3">48.4</td><td colspan="3">60.3</td><td colspan="3">4.5</td><td colspan="3">8.5</td></tr>
</table>

In this model, mesh sensitivity analysis was performed for three different element sizes of 5 mm, 10 mm, and 20 mm. Moreover, in the case of solid elements, 8-node Hex elements (C3D8R) were used for slabs and columns, and T3D2 elements were utilized for rebars and fibers. Fig. 5b displays a view of the mesh. In the model, the boundary and loading conditions involved constraining the bottom of the slab and exerting a vertical force on the column, respectively (Fig. 5(c))

### *2.2.1 Finite element modeling in Abaqus*

A comprehensive three-dimensional finite element (FE) model was developed using Abaqus/Standard to simulate the behavior of reinforced concrete (RC) flat slab–column connections strengthened with CFRP plates. The model aimed to replicate the geometry, material behavior, and loading conditions of the reference experimental study by Hamoda and Hossain (2019).

The concrete slab and column were modeled using 8-node linear brick elements with reduced integration (C3D8R), which are well-suited for nonlinear concrete behavior and damage localization. Steel reinforcement bars were represented by 2-node truss elements (T3D2), and the CFRP plates were modeled using 4-node shell elements with reduced integration (S4R), capturing in-plane and bending effects efficiently.

Mesh sensitivity analysis was conducted to determine the optimal mesh size. Finer meshing was applied in the critical zone around the slab–column connection to improve accuracy in capturing stress concentrations and failure initiation.

The Concrete Damaged Plasticity (CDP) model was used to simulate the nonlinear behavior of concrete under compressive and tensile loading, including stiffness degradation and post-cracking behavior. The CDP parameters were calibrated based on experimental data

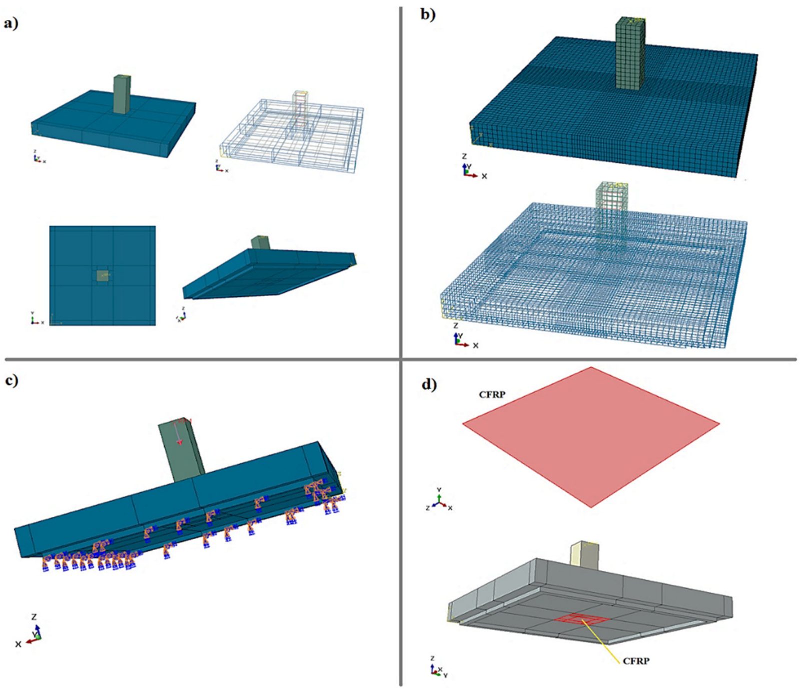


Fig. 5 Specifications of the numerical model: (a) schematic of the slab-column model; (b) finite element model meshing; (c) boundary and loading conditions; (d) CFRP plates in the numerical model

provided in Hamoda and Hossain (2019).

Steel reinforcement was assumed to behave as an elastic–perfectly plastic material with isotropic hardening. The tensile behavior of CFRP was modeled as linear elastic up to failure using the Hashin damage criterion, which captures fiber and matrix cracking modes.

The interaction between concrete and reinforcement bars was modeled using the embedded region technique in Abaqus. In this approach, the rebar elements are fully bonded to the surrounding concrete mesh, assuming no relative slip (perfect bond). Bond–slip behavior was not explicitly considered in this study to reduce model complexity and focus on the global structural response.

The interface between CFRP plates and concrete was modeled using surface-to-surface contact with cohesive behavior to simulate potential delamination under loading. The traction–separation law was defined along with damage initiation and evolution criteria, consistent with the Hashin failure model.

Fixed boundary conditions were applied to the base of the column and the edges of the slab to replicate the experimental support conditions. A monotonic vertical load was applied at the top of the column in displacement control mode. Nonlinear static analysis was conducted using the Static General solver with automatic time stepping and convergence control enabled to handle contact nonlinearity and material softening.

The developed FE model was validated against the experimental results from Hamoda and Hossain (2019). Good agreement was observed in terms of peak load capacity, deflection response, and damage patterns, confirming the accuracy and reliability of the numerical simulation.

In the numerical model developed using Abaqus, different interaction techniques were defined to realistically simulate the behavior of composite components:

- The interaction between concrete and reinforcement bars was modeled using the *embedded region* technique, in which steel rebar elements are embedded into the host concrete elements. This approach assumes a perfect bond between concrete and steel, which is widely accepted in similar numerical studies. Bond-slip behavior was not explicitly modeled, as the primary focus of the study was on evaluating the global structural response and optimizing CFRP strengthening configuration.
- The CFRP–concrete interface was modeled using a *surface-to-surface contact interaction* along with the cohesive behavior defined through the Hashin damage model. This allowed the simulation to account for potential debonding or delamination under loading. Damage evolution and stiffness degradation in the CFRP layers were included using traction-separation laws.

These interaction definitions were selected to achieve a balance between modeling accuracy and computational efficiency while capturing the critical failure mechanisms in the slab–column connection.

### *2.3 Evaluation of the punching shear capacity of the RC slab*

In the design of RC slab-column connections, punching shear capacity is a major design criterion, and guidelines and regulations have introduced various relationships for calculating this quantity. The punching shear capacity can be determined in two directions using the guidelines recommended by international building design regulations and standards. The equations presented in ACI-318, BS-8110, Eurocode 2, and CSAS806 are often used to compute the ultimate strength in concrete slabs. Theoretically, the ACI and CSA-S806 standards provide a conservative design for punching by considering the nearest distance between the critical section and the support and other parameters. However, other standards consider the critical distance to be longer than d/2-2d for design based on punching shear strength. Accordingly, the present research used the equations in ACI-318 to evaluate the punching shear capacity ($V_c$) (Hamoda and Hossain 2019).

$$V_1 = 0.33\lambda\sqrt{f_c}b_0 d \tag{1}$$

$$V_2 = (0.17 + \frac{0.34}{\beta_0})\lambda\sqrt{f_c}b_0 d \tag{2}$$

$$V_3 = 0.083(2 + \frac{\alpha_s d}{b_0})\lambda\sqrt{f_c}b_0 d \tag{3}$$

$$V_c = min(V_1, V_2, V_3) \tag{4}$$

In Eqs. (1)-(4), $f_c$ represents the cylinder compressive strength of concrete, $\lambda$ is the shear reduction factor in concrete, $\beta_0$ is the ratio of the larger side to the smaller side of the concrete column, $b_0$ denotes the critical shear perimeter of the slab located at a distance of 0.5d from the column, and $\alpha_s$ is the location factor of the column, which is equal to 4 for internal columns, 3 for edge columns, and 2 for corner columns. Also, d represents the effective length of the concrete (Hamoda and Hossain 2019).

### *2.4 Numerical models*

In this research, parametric studies were conducted to evaluate the effect of CFRP plates by varying the four main parameters, namely loading conditions, CFRP plate thickness, CFRP plate dimensions, and number of layers and fiber orientation in the CFRP plates. In this regard, numerical modeling approaches were defined by considering the variables under study (classified in the following), and parametric studies were performed to determine the effect of CFRP plates in strengthening slab-column connections in Abaqus software. Table 4 presents the main variables along with the modeling parameters and conditions for each variable.

Based on the scenarios, the slab-column connection was numerically simulated under static and cyclic (seismic) loading. In this research, the ATC-SAC loading protocol (Krawinkler *et al*. 2000) was used to apply cyclic loading. This protocol is related to far-fault earthquakes. Moreover,

Table 4 Variables in the numerical study

| | |
|---|---|
| **Loading conditions** | Static loading<br>Seismic loading |
| **CFRP plate thickness** | Type 1 (T1): thickness of 1 mm<br>Type 2 (T2): thickness of 2 mm<br>Type 3 (A3): 400 mm × 400 mm |
| **CFRP plate dimensions** | Type 1 (A1): 200 mm × 200 mm<br>Type 2 (A2): 100 mm × 100 mm<br>Type 3 (A3): 400 mm × 400 mm |
| **Number of layers and fiber orientation in the CFRP plates** | Type 1 (L1): one layer with a fiber orientation of 0°<br>Type 2 (L2): one layer with a fiber orientation of 90°<br>Type 3 (L3): four layers with a fiber orientation of 0°,45°,90°,0°<br>Type 4 (L4): four layers with a fiber orientation of 45°,90°,0°,45°<br>Type 5 (L5): four layers with a fiber orientation of 90°,0°,45°,90° |

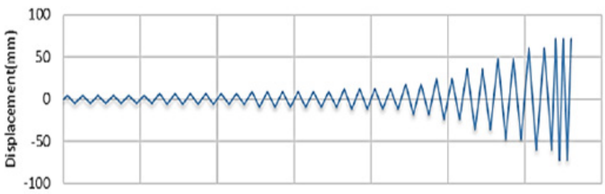


Fig. 6 SAC seismic loading protocol

in this protocol, the displacement is applied at the end of the column according to the loading history, including incrementally increasing cyclic deformations. The SAC cyclic loading protocol is displayed in Fig. 6. A total of 33 numerical models (M1-M33) consisting of different combinations of the main variables was defined and implemented in Abaqus for evaluating the effect of the CFRP plate parameters on the strengthening of slab-column connections.

#### *2.4.1 Definition of damage index and its use in optimization*

In this study, the damage index used as the objective function in the optimization process is extracted directly from the finite element simulation outputs of Abaqus. Specifically, the DAMAGET variable, which is part of the Concrete Damaged Plasticity (CDP) model, is utilized.

DAMAGET is a scalar field variable in Abaqus that represents tensile damage in concrete. It ranges from 0 (no damage) to 1 (complete failure in tension). This parameter is computed at integration points and reflects the progressive stiffness degradation of the concrete under tensile loading due to cracking. According to the Abaqus User Guide (Abaqus Documentation 2020), the relationship between the undamaged and damaged stiffness is defined as

$$E_d = (1 - d_t).E_0 \tag{5}$$

Where:

- $d_t$ is the DAMAGET variable (tensile damage index)
- $E_0$ is the initial elastic modulus of concrete
- $E_d$ is the degraded modulus after tensile cracking

This relationship shows that DAMAGET directly quantifies the extent of material degradation under tensile loads, making it a reliable indicator of structural damage in simulations.

Thus, the variable DAMAGET effectively quantifies the loss of stiffness due to tensile cracking, making it a physically meaningful and computationally reliable damage indicator.

During the optimization process, the maximum value of DAMAGET within the slab–column connection zone is extracted after each simulation run. This value is then fed into the GWO algorithm implemented in MATLAB as the objective function, which the optimizer attempts to minimize.

By minimizing DAMAGET, the algorithm effectively searches for the CFRP design configuration that results in minimal tensile degradation and improved structural performance under loading.

The use of DAMAGET as a numerical damage indicator is widely supported in the literature. It has been employed in various structural simulation and optimization studies to represent damage accumulation in concrete:

- Lee and Fenves (1998): The original developers of the CDP model used internal damage variables as indicators of tensile and compressive failure progression.
- Jankowiak and Lodygowski (2005): Utilized DAMAGET and DAMAGEC to model fracture propagation in concrete elements.
- Minafò *et al.* (2017) and González-Vidosa *et al.* (2020): Used CDP damage variables in flat slab punching shear failure analysis and damage-based design methods.

These references confirm that DAMAGET is theoretically sound, physically meaningful, and computationally efficient for use as a performance criterion in optimization-driven design.

### *2.4.2 Failure criteria in the FEM Model*

A reliable failure definition was implemented in the numerical model to accurately simulate the fracture mechanisms of the RC slab-column connection and its strengthened variants. The failure of each component—concrete, reinforcement, and CFRP—was modeled using appropriate constitutive laws and damage evolution strategies as follows:

The Concrete Damaged Plasticity (CDP) model was used to simulate cracking and crushing of concrete. Tensile and compressive degradation were monitored using the Abaqus scalar variables DAMAGET and DAMAGEC, respectively.

- Tensile cracking was assumed to initiate when the tensile stress reached the tensile strength of the material.
- Complete tensile failure was considered when DAMAGET → 1.0.
- Similarly, compressive failure was associated with DAMAGEC → 1.0, signifying full material degradation in compression.

The reinforcement bars were modeled as elastic–perfectly plastic, using a bilinear stress–strain relationship with:

- Yield stress fy = 365 MPa
- Ultimate strain based on code-based steel behavior
- Failure assumed when the strain exceeded the fracture limit (as defined in the experimental reference)

No bond-slip was modeled between the reinforcement and concrete (embedded region approach was adopted), so bar failure corresponds to reaching the plastic strain limit.

Failure in CFRP laminates was evaluated using the Hashin failure criterion, integrated into the finite element model through the damage initiation and evolution laws. Four modes of failure were considered:

1. Fiber tension failure
2. Fiber compression failure
3. Matrix tension failure
4. Matrix compression failure

Damage initiation triggers stiffness degradation in each failure mode, and the material was considered failed when any of the Hashin criteria reached their limit state. This multi-criteria approach allowed accurate simulation of progressive failure and delamination in the CFRP-strengthened regions.

### *2.5 GWO algorithm*

The GWO algorithm is among population-based metaheuristic algorithms and was inspired by the pack-hunting behavior of wolves (Truong *et al*. 2022). Based on the hierarchy in the social life of gray wolves, the alpha (α) wolf leads the pack and is responsible for deciding on hunting, sleeping location, time of movement, etc. The second rank in the hierarchy is occupied by beta (β) wolves. These wolves are under the alpha wolves' command and help them in their decision and other activities of the pack. Beta wolves are the best candidates for an alpha wolf and act as deputies for alpha wolves and as regulators for the pack. The lowest rank in the hierarchy belongs to omega (ω) wolves. These wolves sacrifice themselves for other pack members. They are the last to feed. If a wolf is not an alpha, beta, or omega, it will be a subordinate or delta (δ) wolf. Delta wolves obey alpha and beta wolves and rule omega wolves. For mathematically modeling the social governance of wolves in the GWO algorithm, the worthiest solution is designated the α solution. The second and third best solutions are named β and δ solutions. The remaining solutions are assumed to be ω solutions. Hence, in the GWO algorithm, the optimization is led by the α, β, and δ solutions, and the ω solutions follow these three groups. In this research, the GWO algorithm was implemented based on pack hunting in wolves, including the searching, encircling, and attacking steps. The following presents each of these steps along with their mathematical relationships.

<u>Searching step:</u> This step involves tracking, chasing, and approaching the prey. The equations for this step are as follows

$$\vec{D} = |\vec{C}.\overrightarrow{X_P}(t) - \vec{X}(t)| \tag{6}$$

$$\vec{X}(t+1) = \overrightarrow{X_P}(t) - \vec{A}\vec{D}| \tag{7}$$

In Eqs. (6)-(7), t represents the current iteration, A and C are coefficient vectors, Xp denotes the prey position vector, and X is the position vector of a gray wolf.

$$\vec{A} = 2\vec{a}.\vec{r_1} - \vec{a} \tag{8}$$

$$\vec{C} = 2\vec{r_2} \tag{9}$$

In Eq. (8), the *a* components decrease linearly (from 2 to 0) as the number of iterations increases, and $r_1$ and $r_2$ are random vectors between 0 and 1. A gray wolf at Position (X,Y) can update its position based on that of the prey (X*,Y*). Based on this algorithm, various locations around the best solution can be obtained by adjusting the values of the A and C vectors (Fig. 7).

Encircling step: This step involves pursuing, encircling, and harassing the prey until it stops.

$$\begin{aligned} \overrightarrow{D_\alpha} &= |\overrightarrow{C_1}\,\overrightarrow{X_\alpha} - \vec{X}| \\ \overrightarrow{D_\beta} &= |\overrightarrow{C_2}\,\overrightarrow{X_\beta} - \vec{X}| \\ \overrightarrow{D_\delta} &= |\overrightarrow{C_3}\,\overrightarrow{X_\delta} - \vec{X}| \end{aligned} \tag{10}$$

$$\begin{aligned} \overrightarrow{X_1} &= \overrightarrow{X_\alpha} - \overrightarrow{A_1}.(\overrightarrow{D_\alpha}) \\ \overrightarrow{X_2} &= \overrightarrow{X_\beta} - \overrightarrow{A_2}.(\overrightarrow{D_\beta}) \\ \overrightarrow{X_3} &= \overrightarrow{X_\delta} - \overrightarrow{A_3}.(\overrightarrow{D_\delta}) \end{aligned} \tag{11}$$

$$\bar{X}(t+1) = \frac{\bar{X}_1 + \bar{X}_2 + \bar{X}_3}{3} \tag{12}$$

Gray wolves are able to detect the location of the prey and encircle it. The hunting is usually led by the alpha wolves. Beta and delta wolves may sometimes participate in

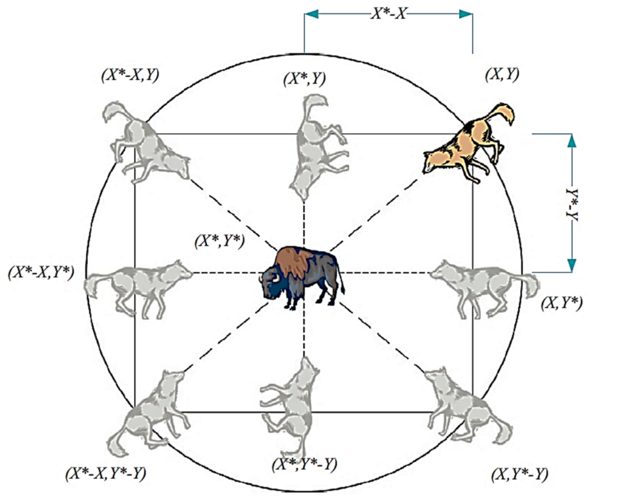


Fig. 7 GWO algorithm; position vectors and updates in the positions of the wolves

hunting. Nevertheless, there is no idea about an optimal (prey) location in a limited search space. For a mathematical simulation of the hunting behavior of gray wolves, it is assumed that alpha (the best solution) beta, and delta are well-informed about the potential prey location. Therefore, the best 3 solutions obtained so far are stored, and the other search agents are forced to update their positions based on those of better agents (Eqs. (10)-(12)).

Attacking step: This step involves a sudden attack on the prey. Gray wolves end hunting by attacking the prey when it has stopped moving. For the purpose of mathematical expression, approaching the prey is implemented by reducing the value of a, where the fluctuation range of vector A also decreases with a. In other words, a is a random value in the range [-2a, 2a], where a decreases from 2 to 0 as the number of iterations increases. When random values of A are within the range [-1, 1], the subsequent position of a search agent can be anywhere between its current position and the position of the prey.

In order to implement the GWO algorithm, the number of search agents (i.e., wolves) and the number of iterations must be determined. Next, the optimization model is implemented based on the GWO algorithm and the presented relationships and determines the optimized values for each variable in the main optimization equation.

#### 2.5.1 Implementation and evaluation of the GWO algorithm

The Grey Wolf Optimizer (GWO) algorithm was implemented in MATLAB and integrated with the Abaqus numerical model for optimal design of CFRP plates. The optimization process was based on minimizing the damage index of RC slab-column connections under static and seismic loading. The initial parameters of the GWO algorithm were set as follows:

- Population size (search agents): 30 wolves
- Maximum iterations: 250
- Stopping criterion: fixed iteration limit

The algorithm was executed multiple times (5 runs) to ensure stability and robustness of the solution. Across all runs, the results converged to similar optimal values for the design variables, with less than 2.5% variation in the final objective function values, indicating high solution consistency.

The algorithm was executed five independent times to ensure stability and robustness of the solution. This number of runs is considered sufficient and has been widely adopted in structural optimization studies employing metaheuristic algorithms, particularly when the numerical model is computationally intensive (e.g., Abaqus simulations) (e.g., Yazdani *et al*. 2022, Emmanuel *et al*. 2022). Across all runs, the results converged to similar optimal values for the design variables, with less than 2.5% variation in the final objective function values, indicating high solution consistency and the convergence history of the GWO algorithm is illustrated in Fig. 19, showing the evolution of the objective function over 250 iterations. The algorithm rapidly reduced the objective function within the first 50 iterations (approximately 80% reduction), and gradually approached a near-optimal solution, stabilizing around iteration 190 with a damage index of approximately 10.7.

This convergence trend demonstrates a balanced exploitation and exploration capability of the GWO algorithm, consistent with the behavior reported in other engineering applications (Mirjalili *et al*. 2014, Emmanuel *et al*. 2022).

While it is acknowledged that metaheuristic algorithms like GWO are susceptible to getting trapped in local optima, the problem was mitigated through:

- A diverse initial population, with random initialization of all variables within defined bounds
- A sufficiently large number of iterations (250) to allow adequate exploration
- Multiple executions, confirming solution stability

No additional hybridization or mutation techniques were applied, as the GWO algorithm demonstrated adequate performance and convergence within the design space of this study.

These observations support the efficiency and reliability of the GWO-based optimization model in identifying globally optimal CFRP configurations for strengthening RC slab-column connections.

### 2.6 Optimization model

In this research, a model was developed using the metaheuristic GWO algorithm in order to obtain optimal values for the geometric parameters of CFRP plates with the aim of strengthening RC slab-column connections. In general, in an optimization process based on the major objectives of the problem (single-objective or multiple-objective optimization), one or more main equations are required, where the main objective of the model is to optimize (minimize or maximize) the values in the main equation(s). In addition, the bounds of the variables in the main equation must be determined. Also, the optimization constraints, which are normally based on the design limitations and requirements, are considered in the form of equations in the optimization model. The main objective of

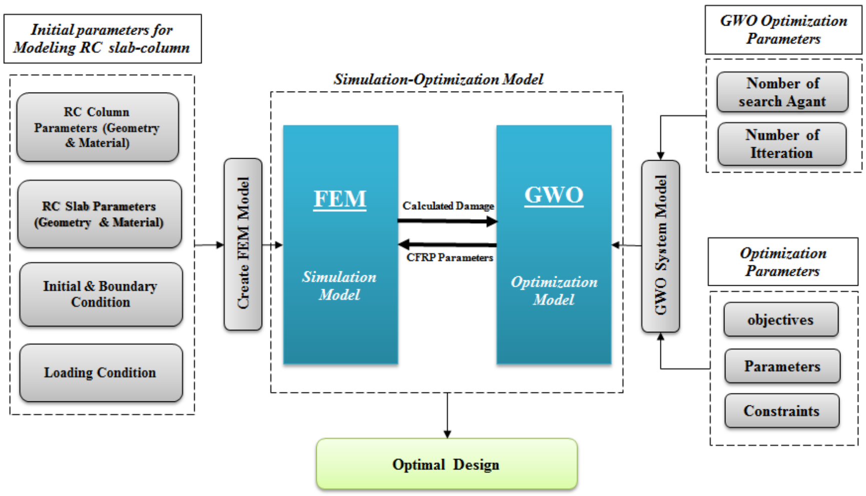


Fig. 8 A schematic of the CFRP optimization model for strengthening a slab-column connection

the optimization model of this research was to reduce damage to CFRP-strengthened slab-column connections under static and seismic loads.

The strategy suggested for the optimal design of CFRP plates for strengthening slab-column connections involves a finite element model of damage in the specimen (slab-column connection) and a computational model for implementing the GWO algorithm and extracting the optimal values of the CFRP plate parameters. Hence, the main equation was implemented in every computational step based on the finite element model and by simulating damage in the specimen. Moreover, the initial value of each CFRP plate parameter, namely plate thickness, plate dimensions, number of layers, and fiber orientation angle, were determined in the computational model in MATLAB. The finite element model was developed in Abaqus, and the computational model was developed in MATLAB using the GWO algorithm. Finally, the two parts of the model were linked. In each computational step, the selected CFRP plate parameter values were input to the finite element model, and the results, including damage values based on loading conditions, were input to the computational model. In the end, the values of the 4 variables of the CFRP plates optimized for strengthening the slab-column connection were extracted. The flowchart in Fig. 8 represents the computational-modeling procedure of the research.

Although the optimization in this study was formulated based on the tensile damage index (DAMAGET) derived from the Concrete Damaged Plasticity (CDP) model, we acknowledge the engineering value of bearing capacity as a direct and physically interpretable performance indicator. However, it is important to note that the DAMAGET variable provides a robust and computationally efficient indicator of degradation, especially in regions where concrete cracking governs failure. It is directly associated with stiffness reduction and progressive failure in tensile zones, which are critical in slab–column connections under vertical or cyclic loading.

Several peer-reviewed studies (e.g., Lee and Fenves 1998, Jankowiak and Lodygowski 2005, Minafò *et al*. 2017, González-Vidosa *et al*. 2020) have successfully employed DAMAGET or its derivatives as surrogate damage metrics in finite element-based optimization and damage assessment frameworks. Furthermore, in this study, the concrete damage index was observed to correlate closely with key structural responses such as crack initiation, ultimate load drop, and CFRP delamination. This confirms that minimizing DAMAGET indirectly enhances global load-carrying capacity and ductility.

Nonetheless, in future studies, we plan to expand the optimization framework into a multi-objective formulation that integrates both DAMAGET and peak bearing capacity as competing objectives. This will enable a more comprehensive balance between minimizing internal damage and maximizing global structural performance, thus enriching the reliability of the design.

## 3. Results and discussion

This section presents and discusses the outcome of the numerical models. For this purpose, the results of validating the numerical model using the experimental model are presented first. Subsequently, the results of the parametric studies on the performance of the CFRP-strengthened slab-column connections are examined. Finally, the performance of the optimal design model developed based on the GWO algorithm is studied.

### *3.1 Experimental model results*

In order to evaluate the performance of the numerical model and validate its results, this section compares the numerical and experimental results. Furthermore, a mesh independence analysis is performed with element sizes of 5 mm, 10 mm, and 20 mm in order to calibrate the numerical model. The results were obtained based on values of (1) crack initiation critical force ($P_{cr}$ $(KN)$) (slab damage) and (2) final crack force ($P_U$ $(KN)$) (slab damage) for various mesh sizes, as shown in Table 5.

Table 5 represents the performance results of the numerical model based on three different mesh sizes and

Table 5 Results of calibrating the numerical model with respect to mesh size

| | Experimental model | Numerical model | | |
|---|---|---|---|---|
| | | Mesh size: 5 mm | Mesh size: 10 mm | Mesh size: 20 mm |
| $P_{cr}$ $(KN)$ | 44 | 42 | 42 | 40 |
| $P_U$ $(KN)$ | 177 | 172 | 171 | 165 |
| **Error %** | - | 3.68% | 3.96% | 7.93% |

compares the error relative to the experimental results. Based on these results, the average computational error of the numerical models with element sizes of 5 mm and 10 mm was about 4%, and that of the model with an element size of 20 mm was around 8%. Moreover, the results indicate no change in the modeling error with a decrease in mesh size from 10 mm to 5 mm. According to the sensitivity analysis, the numerical model was generated with a mesh size of 10 mm, and the studies were conducted based on this model.

After the mesh size was determined, the laboratory model of Hamoda and Hossain (2019) was modeled in Abaqus with all its details and experimental setup, and the numerical modeling results, namely the deflection of the slab and column under the loading conditions, stress distribution in the slab, and damage in the slab, were examined. Fig. 9 displays the slab deflection.

Fig. 10 shows the stress distribution in the concrete slab under loading conditions (based on the experimental model). In this figure, the stress distribution patterns at the surface, cross section, and flat concrete slab rebars are displayed. Fig. 11 presents an evaluation of the vulnerability of the concrete slab under experimental conditions. The results were discussed in terms of the performance of the numerical model. In order to evaluate the performance of the numerical model, the experimental results were compared to the numerical results obtained from Abaqus. To this end, the values of the deflection in the model based on loading and the strain created in the slab rebars based on loading were compared. The graphs of Figs. 12 and 13 show the deflection versus the load in the model and strain in the compressive slab rebars versus load, respectively, in the experimental-numerical test based on the research by Hamoda and Hossain (2019).

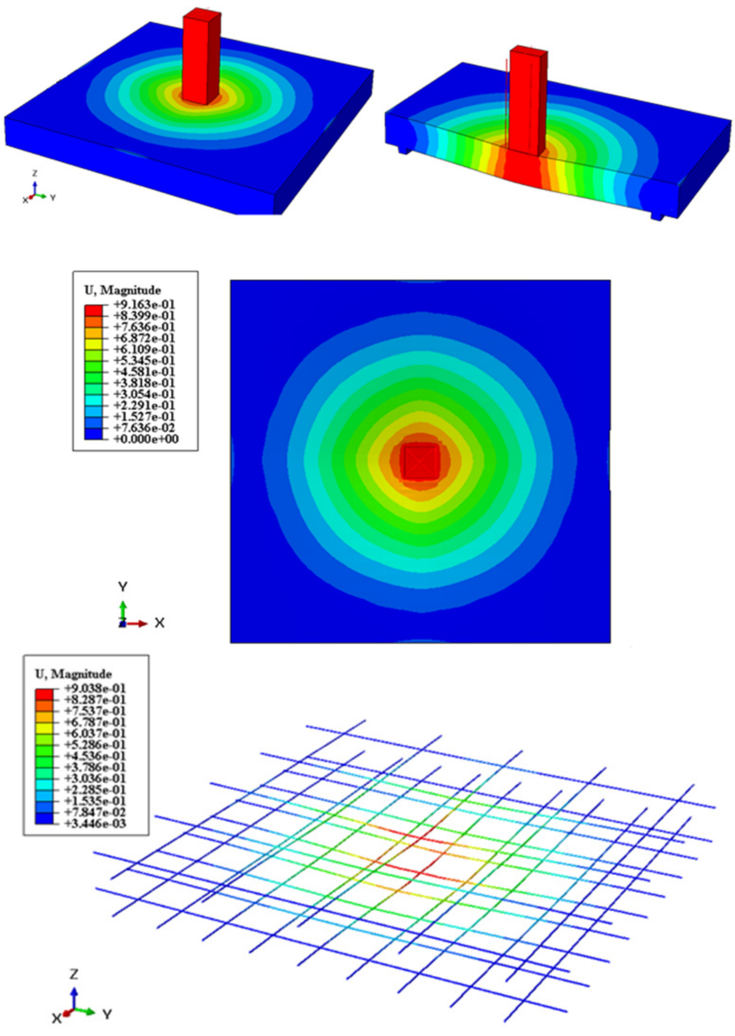


Fig. 9 Numerical results of the laboratory model: deflection

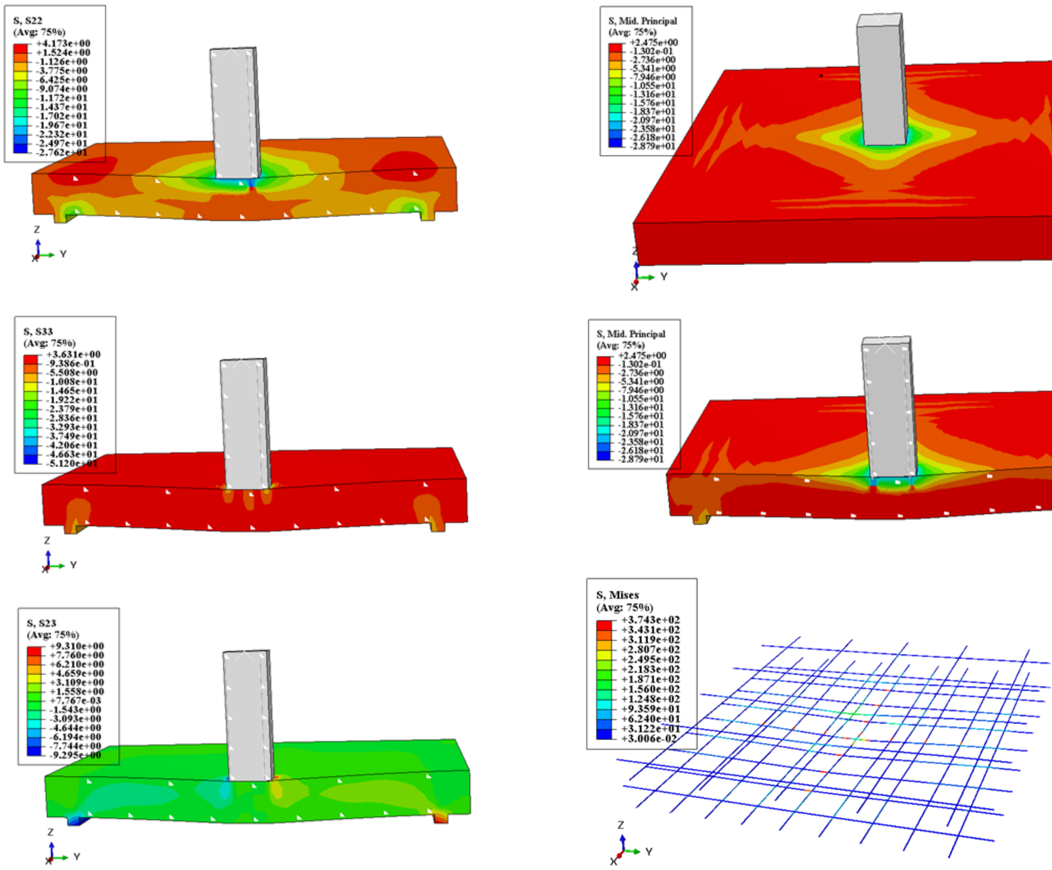


Fig. 10 Numerical results of laboratory model: stress distribution patterns

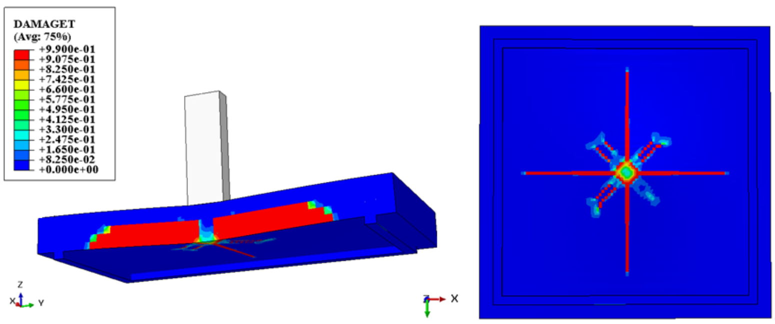


Fig. 11 Numerical results of laboratory model: Vulnerability evaluation of the RC slab

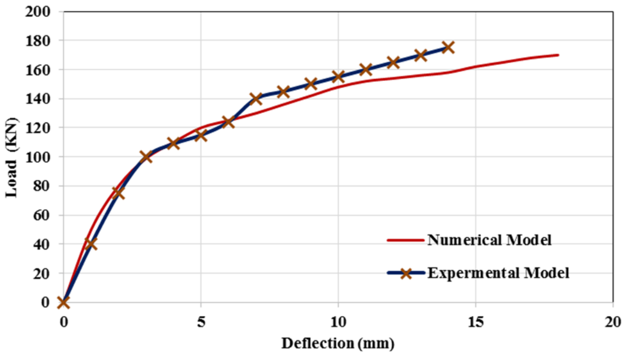


Fig. 12 Comparison of the numerical and experimental results: slab deflection versus load

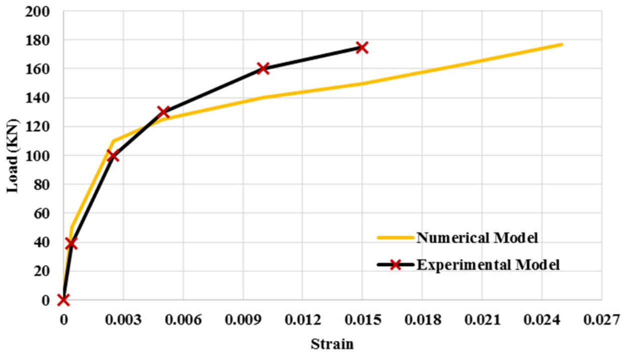


Fig. 13 Comparison of the numerical and experimental results: rebar strain versus load

Table 6 Comparison of the numerical and experimental results for the slab-column connection

| **Parameter/model** | $P_{cr}$ $(KN)$ | $\Delta_{cr}$ $(mm)$ | $P_U$ $(KN)$ | $\Delta_U$ $(mm)$ |
|---|---|---|---|---|
| Experimental model | 44 | 0.74 | 177 | 12.48 |
| Numerical model | 42 | 0.68 | 171 | 11.9 |
| Error | 4.5% | 8.1% | 3.38% | 4.65% |
| Total average modeling error | 5.2% | | | |

The comparison between the numerical and experimental results indicates that the numerical had acceptable accuracy. Moreover, a comparison was performed between the crack initiation parameters in the numerical model and the experiment, the results of which along with the related error in the numerical model are displayed in Table 6. Main parameters under study: (1) crack initiation critical force (slab damage) ($P_{cr}$ $(KN)$); (2) deflection (crack length) ($\Delta_{cr}$ $(mm)$); (3) final crack force (slab damage) ($P_U$ $(KN)$); (4) final deflection corresponding to final crack force ($\Delta_U$ $(mm)$)

### *3.2 Parametric study*

The parametric studies aimed to examine the impact of the modeling variables, namely loading conditions, CFRP plate thickness, CFRP plate dimensions, and number of layers and fiber orientation, on the strengthening of RC slab-column connections using CFRP plates. The numerical modeling approaches were defined based on the modeling variables. The following presents and discusses the results on a case-by-case basis.

### *3.2 The effect of the number of layers in CFRP*

In the first and second models (M1 and M2), the slab-column connection was simulated with a single-layer plate under punching shear load conditions in order to assess the effect of CFRP plates. In these two models, the fiber orientation angles were 0 and 90°. The modeling results representing the level of damage in the concrete slab are shown in Fig. 14.

Based on the comparison between the numerical and experimental results (unstrengthened model), using CFRP plates can reduce damage to slab-column members and improve their behavior under various loading conditions (reduction in punching shear and radial cracks). Therefore, for the parametric studies, the CFRP plates were considered to have 4 layers and (0, 45°, 90°) fiber orientation angles. Hence, after extensive modeling, comprehensive parametric studies were conducted based on the main variables of CFRP plates, and the damage level in the slab-column connection was evaluated as the criterion for comparing different models.

### *3.2.2 Effect of fiber orientation in CFRP plates*

In order to evaluate the effect of fiber orientation in CFRP plates, three models with identical dimensions (200 mm × 200 mm × 1 mm) and different fiber orientations (of fibers L3, L4, and L5 according to Table 4) were created. For assessing the performance of the CFRP plates, the strain energy and slab damage were examined in the three models. Fig. 15 shows the changes in the strain energy and slab damage versus the load and compares the maximum

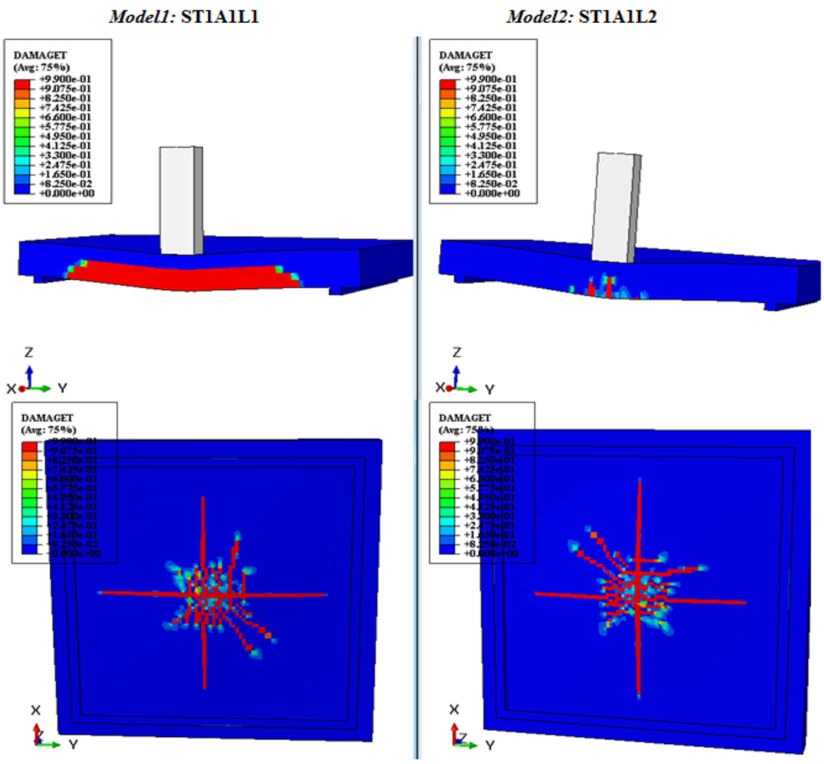


Fig. 14 Slab vulnerability assessment in tensile elements strengthened with single-layer CFRP plate

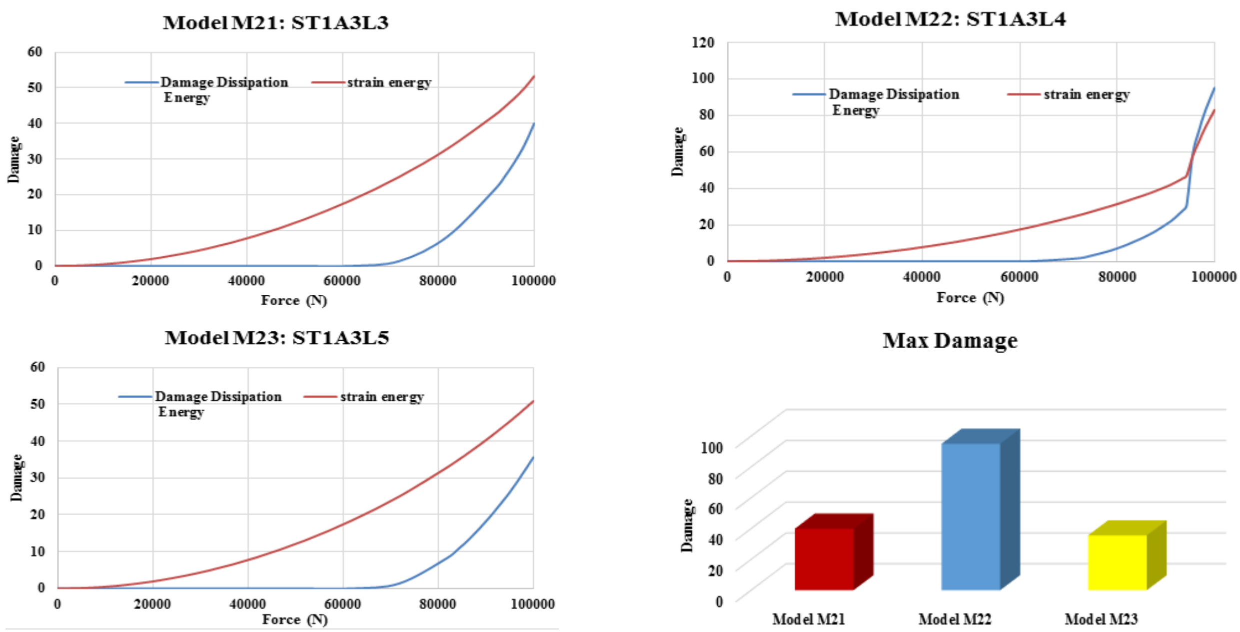


Fig. 15 Sensitivity analysis results of fiber orientation in CFRP plates

damage in the three models. In each graph, the red curve represents the variations in strain energy, while the blue curve represents the changes in damage level with changes in load.

Based on the results, the M3 and M5 models exhibited better performance than the M4 model. In the three models, the only variable was the fiber orientation. As seen in the results, the fiber orientation of L3: (0,45,90,0) produced a better performance compared to L4 and L5. Furthermore, for examining the effect of the CFRP plate thickness (T) and dimensions (A), models were generated with identical CFRP plate thickness and dimensions and different fiber orientations. In this research, the influence of fiber orientation in the CFRP plate was studied under three different conditions, namely L3 with fiber orientations of (0,45,90,0) and four layers L4 with fiber orientations of (45, 90, 0, 45) in four layers, and L5 with fiber orientations of (90, 0, 45, 90) in four layers. Based on previous discussions and the numerical results, the best strengthening behavior was achieved under L3 conditions. In other words, the least damage occurred in the concrete slab when the CFRP plate had 4 layers with fiber orientations of (0,45,90,0).

### *3.2.3 Effect of CFRP plate thickness*

In this study, the influence of CFRP plate thickness on strengthening the slab-column connection was investigated under three conditions: T1, T2, and T3 with CFRP plate thicknesses of 1 mm, 2 mm, and 3 mm, respectively. According to the fiber orientation results, the best fiber orientation condition was L3. Thus, in order to evaluate the impact of thickness (T), all the models with a fiber orientation of L3, identical dimensions (A), and different thicknesses were compared. These models consisted of three groups: Group 1: M3, M6, and M9 (these models had fiber orientations of L3, dimensions of A1, and different CFRP plate thicknesses); Group 2: M12, M15, and M18

Table 7 Sensitivity analysis of the CFRP plate performance with respect to thickness (T)

| Model | | | |
|---|---|---|---|
| **CFRP plate thickness** | **M3: ST1A1L3 (T1)** | **M6: ST2A1L3 (T2)** | **M9: ST3A1L3 (T3)** |
| Concrete slab damage | 47.9946 | 32.5343 | 697.522 |
| Reduction in damage compared to the original model (%) | 95.48 | 96.93 | 34.28 |
| **CFRP plate thickness** | **M12: ST1A2L3 (T1)** | **M15: ST2A2L3 (T2)** | **M18: ST3A2L3 (T3)** |
| Concrete slab damage | 661.659 | 613.477 | 652.918 |
| Reduction in damage compared to the original model (%) | 37.66 | 42.20 | 38.48 |
| **CFRP plate thickness** | **M21: ST1A3L3 (T1)** | **M24: ST2A3L3 (T2)** | **M27: ST3A3L3 (T3)** |
| Concrete slab damage | 40.0195 | 11.5234 | 12.9486 |
| Reduction in damage compared to the original model (%) | 96.23 | 98.91 | 98.78 |

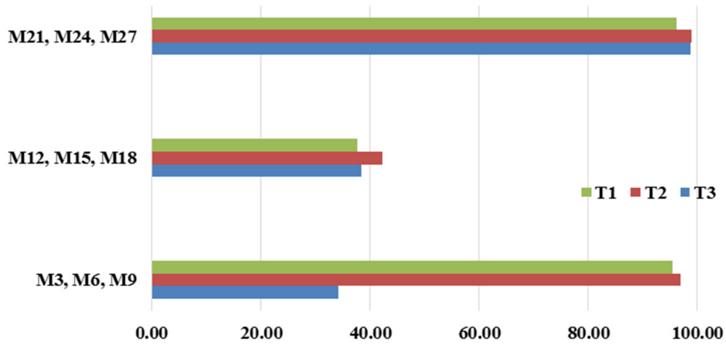


Fig. 16 Study of the role of CFRP plate thickness in damage reduction in the concrete slab

Table 8 Sensitivity analysis of the CFRP plate performance with respect to plate dimensions (A)

| **Model** | | | |
|---|---|---|---|
| **Dimensions A** | **M3: ST1A1L3 (A1)** | **M12: ST1A2L3 (A2)** | **M21: ST1A3L3 (A3)** |
| Concrete slab damage | 47.9946 | 661.659 | 40.0195 |
| Reduction in damage compared to the original model (%) | 95.48 | 37.66 | 96.23 |
| **Dimensions A** | **M6: ST2A1L3 (A1)** | **M15: ST2A2L3 (A2)** | **M24: ST2A3L3 (A3)** |
| Concrete slab damage | 32.5343 | 613.477 | 11.5234 |
| Reduction in damage compared to the original model (%) | 9.93 | 42.20 | 98.91 |
| **Dimensions A** | **M9: ST3A1L3 (A1)** | **M18: ST3A2L3 (A2)** | **M27: ST3A3L3 (A3)** |
| Concrete slab damage | 697.522 | 652.918 | 12.9486 |
| Reduction in damage compared to the original model (%) | 34.28 | 38.48 | 98.78 |

(these models had fiber orientations of L3, dimensions of A2, and different CFRP plate thicknesses); and Group 3: M21, M24, and M27 (these models had fiber orientations of L3, dimensions of A3, and different CFRP plate thicknesses). Table 7 presents the damage parameter comparison between these models.

Table 7 also shows the sensitivity analysis of the CFRP plate performance in strengthening the flat slab-column connection with respect to the plate thickness (T). Based on the results, the largest reduction in slab damage occurred in the models with CFRP plates of thickness T2 = 2 mm. Specifically, the use of CFRP plates with a thickness of T2 led to a 96.93%, 42.2%, and 98.91% decrease in damage in Groups 1, 2, and 3, respectively. Hence, the best thickness for CFRP plates used to strengthen the slab-column connection and reduce damage due to punching shear was found to be 2 mm. An evaluation of the effect of CFRP plate thickness on the percentage reduction of damage in the concrete slab based on the comparison groups is shown in Fig. 16.

### *3.2.4 Effect of CFRP plate dimensions*

In order to study the impact of CFRP plate dimensions on strengthening slab-column connections, three conditions were defined: A1, A2, and A3, corresponding to CFRP plate dimensions of 200 mm × 200 mm, 100 mm × 100 mm, and 400 mm × 400 mm, respectively. According to the results, the best CFRP fiber orientation condition was L3. Hence, models with fiber orientations of L3, identical thickness (T), and different dimensions were compared to determine the effect of dimensions (A). These models consisted of three groups: Group 1: M3, M12, and M21 (these models had fiber orientations of L3, thicknesses of T1, and different CFRP plate dimensions); Group 2: M6, M15, and M24 (these models had fiber orientations of L3, thicknesses of T2, and different CFRP plate dimensions); and Group 3: M9, M18, and M27 (these models had fiber orientations of L3, thicknesses of T3, and different CFRP plate dimensions). Table 8 compares the damage parameter between these models.

Table 8 also shows the sensitivity analysis of the CFRP plate performance in strengthening the flat slab-column connection with respect to the plate dimensions (A). The results indicated that the largest reduction in slab damage occurred in models with CFRP plates of dimensions A3 = 400 mm × 400 mm. Specifically, the use of CFRP plates with dimensions of A3 led to a 96.23%, 98.91%, and 98.78% decrease in damage in Groups 1, 2, and 3, respectively. Hence, the best dimensions for CFRP plates used to strengthen slab-column connections and reduce

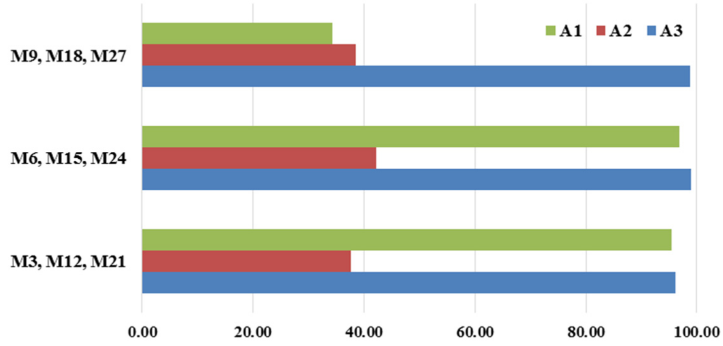


Fig. 17 Evaluation of the effect of CFRP plate dimensions in reducing slab damage

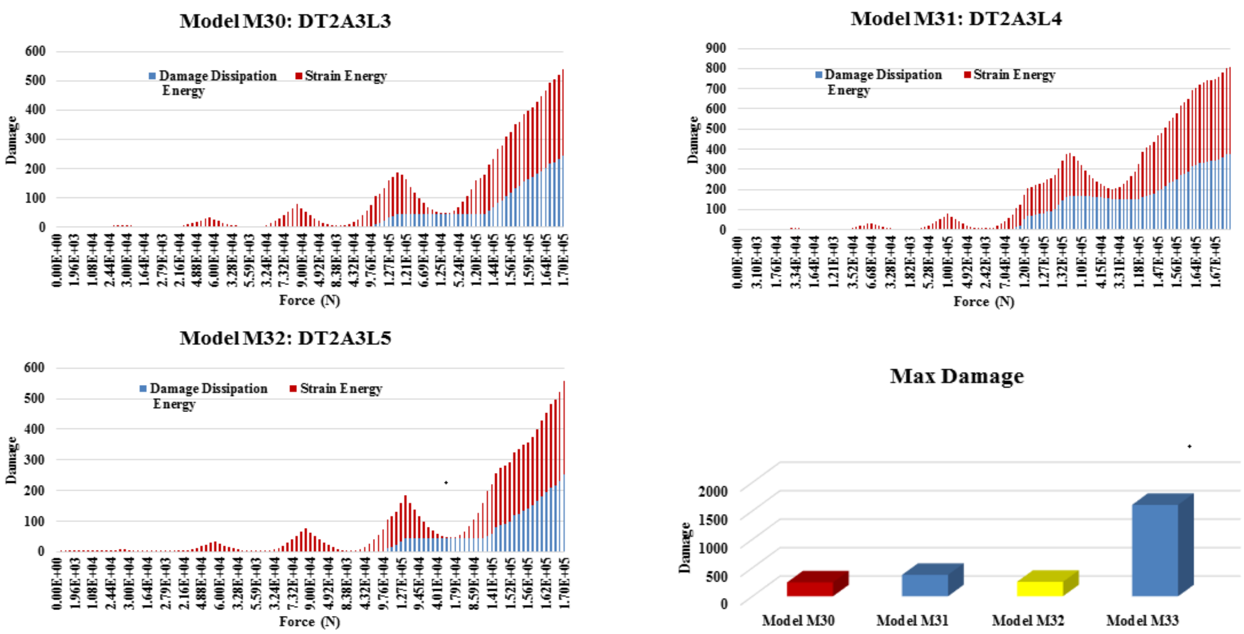


Fig. 18 Performance of the CFRP plates under seismic loading

damage due to punching shear were found to be A3. Fig. 17 examines the effect of CFRP plate dimensions on the percentage reduction of slab damage based on comparisons between the groups.

### 3.2.5 CFRP plate performance under seismic loading

This section presents the performance results of the CFRP plates in strengthening a slab-column connection under seismic loading. According to the numerical results corresponding to punching shear loading, the CFRP plates with a thickness of T2 performed better than those with thicknesses of T1 and T3. In addition, CFRP plates with dimensions of A3 exhibited better strengthening behavior. Accordingly, three numerical models of the slab-column connection with CFRP plates of thickness T2 and dimensions A3 and three fiber orientations (L3, L4, and L5) were simulated under seismic loading conditions. This section presents the results corresponding to Models M30-M33, modeled under seismic loads. Models DT2A3L3, DT2A3L4, and DT2A3L5 involved identical CFRP plate thicknesses of T2 (2 mm) and dimensions of A3 (400 mm × 400 mm) and different fiber orientations in their CFRP plates. Model M33 was the experimental slab-column connection model, which was simulated under seismic loading conditions. The following discusses the damage level in each of these models and compares their performance. In order to evaluate the performances of the CFRP plates under seismic loading, changes in strain energy and slab damage versus load were studied. Fig. 18 shows the variations in the strain energy and slab damage versus the cyclic load. According to the numerical results, the slab damage in all three strengthened models was significantly reduced under seismic loading compared to the original model (slab-column connection without CFRP plates).

A study of the strengthened models under dynamic loading (Fig. 18) indicates that Model M31 showed more damage and strain energy than M30 and M32. Moreover, Model M30 had the best performance in terms of strengthening the slab-column connection under seismic loading. Evaluating the maximum damage in the four numerical models shows that Model M30 performed considerably better than the other two models. The only variable in these three models was the fiber orientation in the CFRP plate, and the results indicate that a fiber orientation of L3 (0, 45, 90, 0) led to better performance compared to L4 and L5 with respect to the RC slab strengthening under seismic loading.

### *3.3 CFRP optimization model*

The optimization model was developed using the metaheuristic GWO algorithm in order to achieve optimal values for the parameters of the CFRP plate with the aim of strengthening RC slab-column connections. The developed model was executed based on the explanations in Section 2 (optimization model). In the optimization model, the main variables whose optimal values were desired and their bounds were as follows:

n: Number of layers of fibers in the CFRP plate (with bounds of $1 \leq n \leq 6$ in the optimization model)

L: Fiber orientation in the CFRP plates (with bounds of $\mathrm{L} = 0°, 45°, 90°$ based on the parametric studies)

T: Thickness of the CFRP plates ($1\ \mathrm{mm} \leq T \leq 4\ mm$)

A: Dimensions of the CFRP plates (this parameter represents the surface area of these plates and has bounds of 10% and 50% of the slab dimensions.) ($100 * 100\ \mathrm{mm} \leq A \leq 500 * 500\ mm$)

Therefore, the developed CFRP optimization model had 4 main variables. Given the explanations provided in Section 2.5, the slab damage was computed in Abaqus software. Accordingly, the main optimization equation is formulated as follows.

$$min(y): \quad Damage = f(n, L, T, A) \tag{13}$$

The initial parameters of the GWO algorithm, namely the number of search agents and the number of iterations, were considered to be 30 and 250, respectively. Table 9 presents the initial values of the variables in the CFRP optimization model.

The developed optimization model was executed, and the damage was calculated by running the finite element model at every step after extracting the initial values of the optimization variables. The damage values computed by the finite element model were input to the model as the solutions to the main optimization equation. Finally, optimal values were obtained for the 4 variables after the completion of the iterations (250). Fig. 19 displays the procedure for obtaining the optimal values during the execution of the CFRP optimization model.

Table 9 Variables of the optimization model and the initial parameters of the GWO algorithm

| Optimization variables | |
|---|---|
| Number of layers in the CFRP plate (n) | $1 \leq n \leq 6$ |
| Fiber orientation in the CFRP palte (L) | $L = 0°, 45°, 90°$ |
| Thickness of the CFRP plate (T) | $1\ \mathrm{mm} \leq T \leq 4\ mm$ |
| Dimensions of the CFRP plate (A) | $100 * 100\ \mathrm{mm} \leq A \leq 500 * 500\ mm$ |
| **GWO parameters** | |
| Number of search agant (SA) | $SA = 30$ |
| Iteration (It) | $It = 250$ |

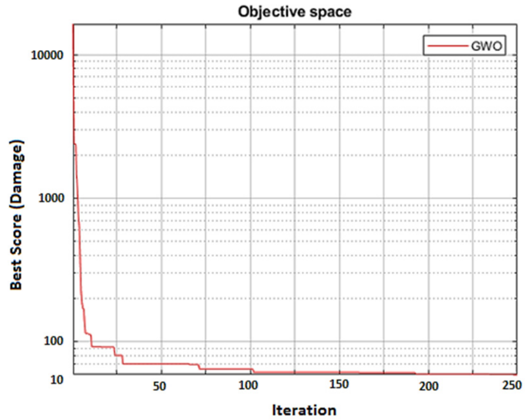


Fig. 19 Optimization procedure for the CFRP plate design

Table 10 Results from the CFRP optimization model

| Optimization model results | |
|---|---|
| $n$ | $n = 5$ |
| $L$ | $L = 0°, 45°, 90°, 0{,}45$ |
| T | T = 2 mm |
| A | A = 400 * 400 mm |
| Damage | 10.7 |

Fig. 12 shows the execution of the CFRP optimization model. As seen in this figure, the solution progress involving the 4 variables of the CFRP plates led to a reduction in the value of the objective function (slab damage). *This value almost stabilized at 10.7 after 190 iterations*. Table 10 presents the results corresponding to the CFRP optimization model, which included optimal values for 4 model variables.

## 4. Conclusions

In this research, comprehensive parametric studies were conducted numerically to evaluate CFRP-strengthening of RC slab-column connections. The main variables were loading conditions (punching shear and seismic), number of layers in the CFRP plate, thickness of the CFRP plate, and fiber orientation in the CFRP plate. Accordingly, 33 modeling solutions were defined and simulated in Abaqus to analyze the sensitivity of the effect of each independent variable. In order to validate the numerical model, an experimental model was used as a basis, and the numerical results underwent verification-validation using the empirical results. The results indicated that the average error of the numerical model relative to the experimental model was 5.2%, demonstrating the acceptable accuracy of the numerical model in evaluating the behavior of the RC slab-column connection.

The results were presented in terms of the slab damage and strain energy in the numerical models. In addition, the damage patterns in the RC slab strengthened with CFRP plates under different loading conditions were presented. Based on the results and the sensitivity analysis of concrete slab strengthening with respect to the variables under study, the fiber orientation in the CFRP plate was found to be an important parameter affecting the behavior of the connection. In addition, the results indicated that the L3 fiber orientation (involving fiber angles of 0°, 45°, 90°, and 0° in four layers) exhibited the best performance in strengthening the RC slab-column connection under both static and seismic loads.

The results also showed that the thickness of the CFRP plates played a significant role in connection strengthening. Moreover, a thickness of T2 (i.e., 2 mm) resulted in the best strengthening performance and the largest reduction in slab damage. Specifically, the use of a CFRP plate with T2 thickness caused 96.93%, 42.2%, and 98.91% reductions in damage compared to the first, second, and third comparison groups. Therefore, the most optimal conditions corresponded to a thickness of 2 mm for the CFRP plates.

The sensitivity of the CFRP plate's performance in strengthening the slab-column connection was analyzed with respect to the plate dimensions (A). Based on the results, the largest damage reduction occurred in models with CFRP plate dimensions of A3 (400 mm × 400 mm). Specifically, the use of a CFRP plate with A3 thickness caused 96.23%, 98.91%, and 98.78% reductions in damage compared to the first, second, and third comparison groups. Hence, the best dimensions for CFRP plates used to strengthen slab-column connections and reduce damage due to punching shear were found to be A3.

In addition to the parametric studies, a model was developed using the metaheuristic GWO algorithm in order to obtain optimal values for the geometric parameters of CFRP plates with the aim of strengthening RC slab-column connections. The model presented for the optimal design of CFRP plates for strengthening slab-column connections involves two main parts: a finite element model representing damage in the connection and a computational model for implementing the GWO algorithm and extracting the optimal values of the CFRP plate parameters.

The finite element model was developed in Abaqus, and the computational model was developed in MATLAB using the GWO algorithm. Finally, the two parts of the model were linked. In each computational step, the CFRP plate parameter values selected in the computational model were input to the finite element model, and the results, including damage values based on loading conditions, were input to the computational model. Based on the results from the CFRP optimization model, the optimal values of the 4 main parameters of the CFRP plates were n = 5 for the number of layers, $L = 0°, 45°, 90°, 0°, 45°$ for the fiber orientation, $T = 2\,mm$ for the plate thickness, and $\mathrm{A} = 400 * 400$ mm for the plate dimensions. Under these conditions, the damage to the RC slab-column connection was minimum and equal to 10.7.

The results of this research can be used as a basis for designing and using CFRP plates to strengthen flat RC slab-column connections. In addition, the CFRP plate optimal design model, developed using the GWO algorithm, can be used practically for the optimal design of these plates. In this study, the developed optimal design model was evaluated by considering 4 geometric-material properties of the CFRP plate. Studies of other variables, such as material properties, dimensions, and initial conditions of the RC slab-column connection based on the model in this research are recommended for future work.

## References


Abaqus Documentation (2020), Concrete Damaged Plasticity – User Guide, Dassault Systèmes.

Abdulrahman, B.Q. and Aziz, O.Q. (2021), "Strengthening RC flat slab-column connections with FRP composites: A review and comparative study", *J. King Saud Univ.-Eng. Sci.*, **33**(7), 471-481. https://doi.org/10.1016/j.jksues.2020.07.005

ACI Committee (2019), Building code requirements for structural concrete (ACI 318-05) and commentary, ACI 318R-05, American Concrete Institute; MI, USA.

Aidy, A., Rady, M., Mashhour, I.M. and Mahfouz, S.Y. (2022), "Structural design optimization of flat slab hospital buildings using genetic algorithms", *Buildings*, **12**(12), p. 2195. https://doi.org/10.3390/buildings12122195

Akhundzada, H., Donchev, T. and Petkova, D. (2019), "Strengthening of slab-column connection against punching shear failure with CFRP laminates", *Compos. Struct.*, **208**, 656-664. https://doi.org/10.1016/j.compstruct.2018.09.076

Al-Kannoon, M.A. and Ali, H.W. (2016), "Strengthening of reinforced concrete solid slabs with CFRP products", *Int. J. Sci. Eng. Res.*, **7**(9), 1237-1243.

Al-Maliki, H.N., Al-Balhawi, A. and Ali, A.M. (2021), "Punching shear resistance of reinforced concrete flat slabs strengthened by CFRP and GFRP: A review of literature", *Eng. Technol. J.*, **39**(8), 1281-1290. http://dx.doi.org/10.30684/etj.v39i8.2011

Al-Rousan, R.Z., Alhassan, M.A. and Al-omary, R.J. (2021), "Response of interior beam-column connections integrated with various schemes of CFRP composites", *Case Stud. Constr. Mater*, **14**, p. e00488. https://doi.org/10.1016/j.cscm.2021.e00488

Aman, S.S., Mohammed, B.S., Wahab, M.A. and Anwar, A. (2020), "Performance of reinforced concrete slab with opening strengthened using CFRP", *Fibers*, **8**(4), p. 25. https://doi.org/10.3390/fib8040025

Anil, Ö., Kaya, N. and Arslan, O. (2013), "Strengthening of one way RC slab with opening using CFRP strips", *Constr. Build. Mater.*, **48**, 883-893. https://doi.org/10.1016/j.conbuildmat.2013.07.093

Azizian, H., Lotfollahi-Yaghin, M.A. and Behravesh, A. (2021), "Punching Shear Strength of Voided Slabs on the Elastic Bases" *Iran. J. Sci. Technol., Transact. Civil Eng.*, **45**, 2437-2449. http://dx.doi.org/10.1007/s40996-020-00546-y

Babiker, A., Abbas, Y.M., Khan, M.I. and Khatib, J.M. (2024), "Improving predictive accuracy for punching shear strength in fiber-reinforced polymer concrete slab-column connections via robust deep learning", *Structures*, **70**, p. 107797. https://doi.org/10.1016/j.istruc.2024.116965

Cai, B., Hao, L. and Fu, F. (2020), "Postfire reliability analysis of axial load bearing capacity of CFRP retrofitted concrete columns", *Adv. Concrete Constr., Int. J.*, **10**(4), 289-299. https://doi.org/10.12989/acc.2020.10.4.289

Cai, Z.W., Liu, X., Li, L.Z., Lu, Z.D. and Chen, Y. (2021), "Seismic performance of RC beam-column-slab joints strengthened with steel haunch system.", *J. Build. Eng.*, **44**, p.

103250. https://doi.org/10.1016/j.jobe.2021.103250

Dada, E., Joseph, S., Oyewola, D., Fadele, A.A., Chiroma, H. and Abdulhamid, S.I.M. (2022), "Application of grey wolf optimization algorithm: recent trends, issues, and possible horizons", *Gazi Univ. J. Sci.*, **35**(2), 485-504. https://doi.org/10.35378/gujs.820885

Daud, R.A. (2015), "Behaviour of reinforced concrete slabs strengthened externally with two-way FRP sheets subjected to cyclic loads", Ph.D. Dissertation; The University of Manchester, Manchester, UK.

Daud, R.A., Cunningham, L.S. and Wang, Y.C. (2015), "Static and fatigue behaviour of the bond interface between concrete and externally bonded CFRP in single shear", *Eng. Struct.*, **97**, 54-67. https://doi.org/10.1016/j.engstruct.2015.03.068

El-Mandouh, M.A., Hu, J.W. and Abd El-Maula, A.S. (2022), "Seismic behavior of RC slab-column connection with openings strengthened with CFRP", *Case Stud. Constr. Mater.*, **17**, p. e01517. https://doi.org/10.1016/j.cscm.2022.e01517

Emmanuel, D.A.D.A., Joseph, S., Oyewola, D., Fadele, A.A. and Chiorma, H. (2022), "Application of grey wolf optimization algorithm: Recent trends, issues, and possible horizons", *Gazi Univ. J. Sci.*, **35**(2), 485-504. http://dx.doi.org/10.35378/gujs.820885

Enochsson, O. (2005), "CFRP strengthening of concrete slabs, with and without openings: experiment, analysis, design and field application", Ph.D. Dissertation; Luleå tekniska universitet, Norrbotten, Sweden.

Esfahani, M.R., Kianoush, M.R. and Moradi, A.R. (2009), "Punching shear strength of interior slab–column connections strengthened with carbon fiber reinforced polymer sheets", *Eng. Struct.*, **31**(7), 1535-1542. https://doi.org/10.1016/j.engstruct.2009.02.021

González-Vidosa, F.G., Kotsovos, M.D. and Pavlovic, M.N. (1988), "Symmetrical punching of reinforced concrete slabs: An analytical investigation based on nonlinear finite element modeling", *ACI Struct. J.*, **85**(3), 241-245.

Haido, J.H., Abdul-Razzak, A.A., Al-Tayeb, M.M., Bakar, B.H., Yousif, S.T. and Tayeh, B.A. (2021), "Dynamic response of reinforced concrete members incorporating steel fibers with different aspect ratios", *Adv. Concrete Constr., Int. J.*, **11**(2), 89-98. https://doi.org/10.12989/acc.2021.11.2.089

Halim, N.H.F.A., Alih, S.C. and Vafaei, M. (2021), "Seismic behavior of RC columns internally confined by CFRP strips", *Adv. Concrete Constr., Int. J.*, **12**(3), 217-225. https://doi.org/10.12989/acc.2021.12.3.217

Hamoda, A. and Hossain, K.M.A. (2019), "Numerical assessment of slab–column connection additionally reinforced with steel and CFRP bars", *Arab. J. Sci. Eng.*, **44**, 8181-8204. https://doi.org/10.1007/s13369-019-03846-2

Harajli, M.H. and Soudki, K.A. (2003), "Shear strengthening of interior slab–column connections using carbon fiber-reinforced polymer sheets", *J. Compos. Constr.*, **7**(2), 145-153. https://doi.org/10.1061/(ASCE)1090-0268(2003)7:2(145)

Jankowiak, T. and Lodygowski, T. (2005), "Identification of parameters of concrete damage plasticity constitutive model", *Found. Civil Environ. Eng.*, **6**, 53-69.

Jayawickrema, M., Kumar, A., Herath, M., Hettiarachchi, N., Sooriyaarachchi, H. and Epaarachchi, J. (2023), "Strain patterns of short span reinforced concrete beams under flexural loading: A comparison between distributed sensing and concrete damaged plasticity modelling", *J. Intell. Mater. Syst. Struct.*, **34**(10), 1123-1135. https://doi.org/10.1177/1045389X221128764

Khalel, H.H.Z. and Khan, M. (2023), "Modelling fibre-reinforced concrete for predicting optimal mechanical properties", *Materials*, **16**(10), p. 3700. https://doi.org/10.3390/ma16103700

Kotynia, R., Walendziak, R., Stoecklin, I. and Meier, U. (2011), "RC slabs strengthened with prestressed and gradually anchored CFRP strips under monotonic and cyclic loading", *J. Compos. Constr.*, **15**(2), 168-180. https://doi.org/10.1061/(ASCE)CC.1943-5614.0000081

Krawinkler, H., Gupta, A., Medina, R. and Luco, N. (2000), "Loading histories for seismic performance testing of SMRF components and assemblies", Report no. SAC/BD-00/10; SAC Joint Venture.

Lee, J. and Fenves, G.L. (1998), "Plastic-damage model for cyclic loading of concrete structures", *J. Eng Mech.*, **124**(8), 892-900. https://doi.org/10.1061/(ASCE)0733-9399(1998)124:8(892)

Liu, H., Wang, Z., Du, X. and Shen, G.Q. (2021), "The seismic behaviour of precast concrete interior joints with different connection methods in assembled monolithic subway station", *Eng. Struct.*, **232**, p. 111799. https://doi.org/10.1016/j.engstruct.2020.111799

Ma, C., Wang, Z. and Smith, S.T. (2020), "Seismic performance of large-scale RC eccentric corner beam-column-slab joints strengthened with CFRP systems", *J. Compos. Constr.*, **24**(2), p. 04019066. https://doi.org/10.1061/(ASCE)CC.1943-5614.0000995

Minafò, G., Brunesi, E., Nascimbene, R. and Casadei, P. (2017), "Numerical modeling of punching shear failure in flat slabs using CDP model", *Eng. Struct.*, **140**, 188-205.

Mirjalili, S., Mirjalili, S.M. and Lewis, A. (2014), "Grey wolf optimizer", *Adv. Eng. Software*, **69**, 46-61. https://doi.org/10.1016/j.advengsoft.2013.12.007

Moon, J., Reda Taha, M.M. and Kim, J.J. (2017), "Flexural strengthening of RC slabs using a hybrid FRP-UHPC system including shear connector", *Adv. Mater. Sci. Eng.*, Article ID 4387545. https://doi.org/10.1155/2017/4387545

Moshiri, N., Czaderski, C., Mostofinejad, D., Hosseini, A., Sanginabadi, K., Breveglieri, M. and Motavalli, M. (2020), "Flexural strengthening of RC slabs with nonprestressed and prestressed CFRP strips using EBROG method", *Compos. Part B: Eng.*, **201**, p. 108359. https://doi.org/10.1016/j.compositesb.2020.108359

Mukhtar, F. and Lardhi, M. (2024), "Punching shear of sustainable recycled aggregate FRC slabs strengthened with NSM FRP bars", *Case Stud. Constr. Mater.*, **21**, p. e03468. https://doi.org/10.1016/j.cscm.2024.106400

Rady, M. and Mahfouz, S.Y. (2022), "Effects of concrete grades and column spacings on the optimal design of reinforced concrete buildings", *Materials*, **15**(12), p. 4290. https://doi.org/10.3390/ma15124290

Rather, A.I., Mirgal, P., Banerjee, S. and Laskar, A. (2023), "Application of acoustic emission as damage assessment technique for performance evaluation of concrete structures: a review", *Practice Period. Struct. Des. Constr.*, **28**(3), p. 03123003. https://doi.org/10.1061/PPSCFX.SCENG-1256

Razavi, S.V., Jumaat, M.Z., EI-Shafie, A.H. and Ronagh, H.R. (2015), "Load-deflection analysis prediction of CFRP strengthened RC slab using RNN", *Adv. Concrete Constr., Int. J.*, **3**(2), 91-102. https://doi.org/10.12989/acc.2015.3.2.091

Salman, W.D., Murtada, A.I. and Qusay, W.A. (2015), "Strengthening of reinforced concrete one-way slabs using CFRP in flexural", *J. Eng. Sci. Res. Technol.*, **4**(8), 2277-9655.

Shi, Q., Ma, G., Guo, J. and Ma, C. (2022), "Punching performance of RC slab-column connections with inner steel truss", *Adv. Concrete Constr., Int. J.*, **14**(3), 195-204. https://doi.org/10.12989/acc.2022.14.3.195

Tan, K.H. and Zhao, H. (2004), "Strengthening of openings in one-way reinforced-concrete slabs using carbon fiber-reinforced polymer systems", *J. Compos. Constr.*, **8**(5), 393-402. https://doi.org/10.1061/(ASCE)1090-0268(2004)8:5(393)

Truong, G.T., Hwang, H.J. and Kim, C.S. (2022), "Assessment of punching shear strength of FRP-RC slab-column connections using machine learning algorithms", *Eng. Struct.*, **255**, p.

113898. https://doi.org/10.1016/j.engstruct.2022.113898

Yagar, A.C., Derogar, S., Ince, C. and Ball, R.J. (2024), "Evaluation of ACI code equation on punching shear strength of slab-column connections strengthened with FRP: A database study", *Eng. Struct.*, **308**, p. 117965. https://doi.org/10.1016/j.engstruct.2024.116740

Yazdani, N., Beneberu, E. and Mohiuddin, A.H. (2018), "CFRP retrofit of concrete circular columns: Evaluation of design guidelines", *Compos. Struct.*, **202**, 458-464. https://doi.org/10.1016/j.compstruct.2018.02.066

Yin, H., Liu, S., Lu, S., Nie, W. and Jia, B. (2021), "Prediction of the compressive and tensile strength of HPC concrete with fly ash and micro-silica using hybrid algorithms", *Adv. Concrete Constr., Int. J.*, **12**(4), 339-354. https://doi.org/10.12989/acc.2021.12.4.339

Yitzhaki, D. (1966), "Punching strength of reinforced concrete slabs", *Journal Proceedings*, **63**(5), 527-542. https://doi.org/10.14359/7637

Zhang, W., Xue, J., Xu, J., Li, B. and Wei, J. (2022), "Bearing capacity assessment of reinforced concrete slab-special-shaped column connections", *Adv. Concrete Constr., Int. J.*, **14**(6), 401-412. https://doi.org/10.12989/acc.2022.14.6.401